PERSPECTIVE

Dalton
www.rsc.org/dalton

Electronic phase separation in transition metal oxide systems †

C. N. R. Rao,* Asish K. Kundu, Md. Motin Seikh and L. Sudheendra
Chemistry and Physics of Materials Unit,
Jawaharlal Nehru Centre for Advanced Scientific Research,
Jakkur P.O., Bangalore –560 064, India

Received 5th May 2004, Accepted 2nd June 2004
First published as an Advance Article on the web 23rd July 2004

Electronic phase separation is increasingly getting recognized as a phenomenon of importance in understanding the magnetic and electron transport properties of transition metal oxides. The phenomenon dominates the rare-earth manganates of the formula $Ln_{1-x}A_xMnO_3$ (Ln = rare earth and A = alkaline earth) which exhibit ferromagnetism and metallicity as well as charge-ordering, depending on the composition, size of A-site cations and external factors such as magnetic and electric fields. We discuss typical phase separation scenarios in the manganates, with particular reference to $Pr_{1-x}Ca_xMnO_3$ (x = 0.3–0.4), $(La_{1-x}Ln_x)_{0.7}Ca_{0.3}MnO_3$ (Ln = Pr, Nd, Gd and Y) and $Nd_{0.5}Sr_{0.5}MnO_3$. Besides discussing the magnetic and electron transport properties, we discuss electric field effects. Rare-earth cobaltates of the type $Pr_{0.7}Ca_{0.3}CoO_3$ and $Gd_{0.5}Ba_{0.5}CoO_3$ also exhibit interesting magnetic and electron transport properties which can be understood in terms of phase separation.

† Based on the presentation given at Dalton Discussion No. 7, 5–7th July 2004, University of St Andrews, UK.

Introduction

Some of the transition metal oxides are known to exhibit compositional and electronic inhomogeneities arising from the existence of more than one phase in crystals of nominally monophasic composition, with the different phases in such materials having comparable compositions. Rare-earth manganates of the general composition, $Ln_{1-x}A_xMnO_3$ (Ln = rare earth and A = alkaline earth), display a variety of effects due to such phase separation giving rise to novel electronic and magnetic properties. The rare-earth manganates became popular because of the colossal magnetoresistance (CMR) exhibited by them.[1–9] CMR and related properties are generally explained on the basis of the double-exchange (DE) mechanism of the electron hopping between the $Mn^{3+}(t_{2g}^3e_g^1)$ and $Mn^{4+}(t_{2g}^3e_g^0)$ ions. Jahn–Teller (J–T) distortion associated with the Mn^{3+} ions and charge-ordering (CO) of the Mn^{3+} and Mn^{4+} ions compete with DE and favour insulating behaviour and antiferromagnetism (AFM).[1] CO in these materials is closely linked to the ordering of the e_g orbitals. Typical of charge-ordered manganates are $Pr_{1-x}Ca_xMnO_3$ (x = 0.3–0.4) and $Nd_{0.5}Ca_{0.5}MnO_3$ which show CO around 250 K and antiferromagnetic ordering (A-type) at

C. N. R. Rao

C. N. R. Rao obtained his PhD from Purdue University and DSc from Mysore University. He is an honorary fellow of the Royal Society of Chemistry and fellow of the Royal Society. His main research interests are in the chemistry of materials.

Asish K. Kundu

Asish K. Kundu obtained his MSc degree in Physics from Banaras Hindu University and is now working for his PhD degree.

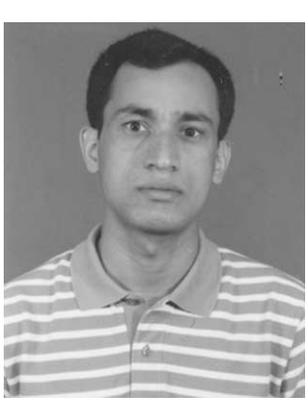

Md. Motin Seikh

Md. Motin Seikh obtained his MSc degree in Chemistry from Visva Bharati University and is now working for his PhD degree.

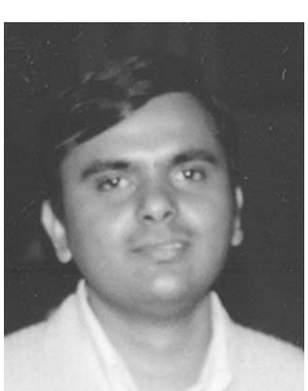

L. Sudheendra

L. Sudheendra obtained his PhD degree from this centre.

DOI: 10.1039/b406785a

lower temperatures. The CO states can be melted into the metallic state by applying high magnetic fields. On the other hand, $Nd_{0.5}Sr_{0.5}MnO_3$ is ferromagnetic below room temperature and shows CO at lower temperatures (~150 K) accompanied by antiferromagnetism (CE-type). The nature of phase separation in the manganates depends on the average size of the A-site cations and the associated size disorder, carrier concentration or the composition (value of x), temperature, and other external factors such as magnetic and electric fields. Phases with different charge densities (carrier concentrations) as well as magnetic and electron transport properties coexist as carrier-rich ferromagnetic (FM) clusters or domains along with a carrier poor antiferromagnetic (AFM) phase. Such an electronic phase separation giving rise to microscopic or mesoscopic inhomogeneous distribution of electrons results in a rich phase diagram.[2] What is noteworthy is that electronic phase separation is likely to be a general property of solids with correlated electrons such as the large family of transition metal oxides. There are indications that many of the unusual magnetic and electron transport properties of oxide materials arise from phase separation.

The term phase separation or segregation implies the presence of at least two distinct phases in the sample, but the relative fractions may vary anywhere from a dilute regime, involving small domains of the minor phase (or clusters) in the matrix of the major phase, to a situation in which the fractions of the two phases are comparable (Fig. 1). Thus, FM clusters present randomly in an AFM host matrix often give rise to a glassy behaviour. As the FM clusters in an AFM matrix grow in size to become reasonably sized domains, due to the effect of temperature, composition, or an applied magnetic field, the system acquires the characteristics of a genuine phase-separated system. In this article, we discuss electronic phase separation and associated effects in magnetic and electron transport properties in rare-earth manganates and cobaltates. The latter system also exhibits ferromagnetism and metallicity when the average size of the cations is sufficiently large and the size disorder is not excessive. The ferromagnetism in the cobaltates is considered to be due to favourable Co^{3+}–O–Co^{4+} superexchange.

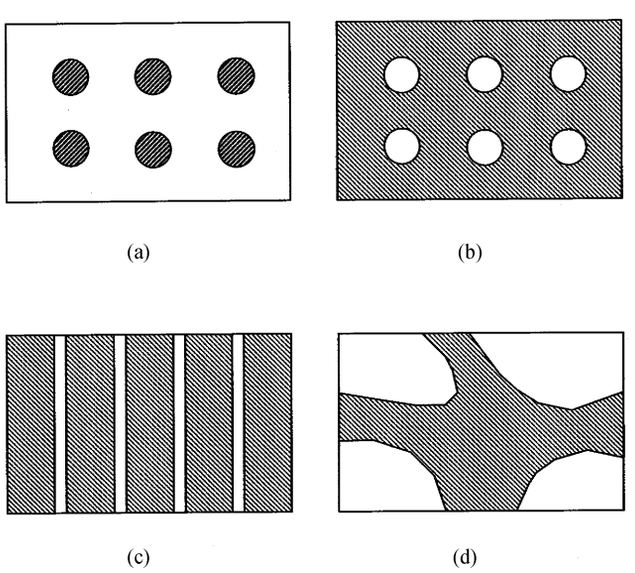

Fig. 1 Microscopic phase-separated state giving rise to (a) an insulating state with ferromagnetic (conducting/metallic) droplets, (b) a conducting state where a ferromagnetic (conducting) part of the crystal has separated (insulating) droplets, and (c) charge-stripes, a macroscopic phase separation state is shown in (d). Hatched portions represent the ferromagnetic regions with high carrier concentration (and are therefore conducting).

Rare-earth manganates

In these materials, the FM phase is conducting and AFM phase is insulating.[2] Depending on x or the carrier concentration, we can have a situation such as that shown in Fig. 1(a) or (b). The phase separation scenario here is somewhat complex because the transition from the metallic to the insulating state is not sharp. In the presence of Coulomb interaction, the microscopically charged inhomogeneous state is stabilized, giving rise to clusters of one phase embedded in another. Electronic phase separation with phases of different charge densities is generally expected to give rise to nanometer scale clusters.[9] This is because large-phase separated domains would break up into small pieces because of Coulomb interactions. The shapes of these pieces could be droplet or stripes (see Fig. 1(a)–(c)). The domains of the two phases can also be sufficiently large to give rise to well-defined signatures in neutron scattering or diffraction.

One can visualize phase separation arising from disorder as well. The disorder can arise from the size mismatch of the A-site cations in the perovskite structure.[3] Such phase separation is seen in the $(La_{1-y}Pr_y)_{1-x}Ca_xMnO_3$ (LPCM) system in terms of a metal–insulator transition induced by disorder. The size of the clusters depends on the magnitude of the disorder. The smaller the disorder, the larger would be the size of the clusters. This could be the reason why high magnetoresistance occurs in systems with small disorder.

Microscopically homogeneous clusters are usually of the size of 1–2 nm in diameter dispersed in an insulating or charge-localized matrix as seen in Fig. 1(a). Such a phase separation scenario bridges the gap between the DE model and the lattice distortion models. Several recent papers on the manganates reveal that in addition to microscopic phase separation, there can be mesoscopic phase separation where the length scale is between 30 and 200 nm, arising from the comparable energies of the FM metallic and AFM insulating states.[1,2,5,9,10] In LPCM and other manganates, the occurrence of multiphases has been observed.[9]

$(La_{1-x}Ln_x)_{0.7}Ca_{0.3}MnO_3$ (Ln = Pr, Nd, Gd and Y)

As mentioned earlier, submicrometer-sized phase separation involving FM and charge-ordered AFM domains has been found in $La_{5/8-y}Pr_yCa_{3/8}MnO_3$. By varying y, the volume fraction and the domain size of the FM and charge-ordered phases can be varied.[9,10] In Fig. 2, we show the results of magnetic measurements [11] on the $(La_{1-x}Nd_x)_{0.7}Ca_{0.3}MnO_3$ series of manganates, to show how the magnetic moment (μ_B) is sensitive to the substitution of the smaller Nd^{3+} cation in place of La^{3+}. We see a clear FM transition down to $x = 0.5$ with a saturation magnetic moment close to $3\mu_B$. The ferromagnetic Curie temperature, T_C, shifts to lower temperature with increase in x. We fail to see magnetic saturation in compositions with $x \geq 0.6$ and, instead, the maximum value of μ_B is far less than 3 at low temperatures. We designate the composition up to which ferromagnetism occurs as the critical composition x_c. The compositions with $x > x_c$ show a gradual, definitive increase in the magnetization or μ_B at a temperature T_M, the T_M value decreasing with increasing x. It is possible that T_M represents the onset of canted antiferromagnetism (CAF). In $(La_{1-x}Gd_x)_{0.7}Ca_{0.3}MnO_3$, ferromagnetism is observed up to $x = 0.3$. The value of T_C decreases with increase in x in the composition range $0.0 \leq x \leq 0.3$. For $x < 0.3$, we observe a gradual increase in the μ_B-value at low temperature around T_M, with the value of T_M decreasing with increase in x. The value of x_c (~0.3) in the Gd series is considerably lower than that in the Nd series where it was 0.6, showing that x_c decreases with the decrease in the average radius of the A-site cation, $\langle r_A \rangle$. The results in the $(La_{1-x}Gd_x)_{0.7}Ca_{0.3}MnO_3$ series of manganates (Fig. 2(b)) obtained by us agree with those reported for the x = 0.0–0.25 compositions by Terashita and Neumeier.[12]

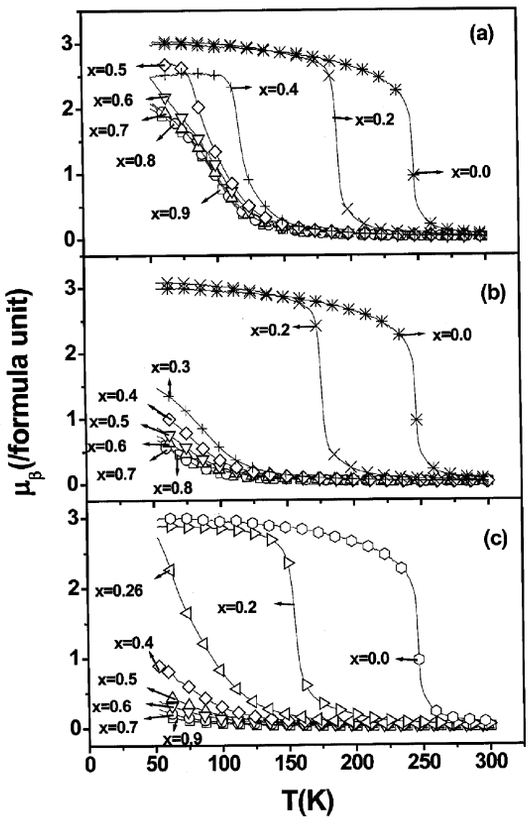

Fig. 2 Temperature variation of μ_B in the manganates (a) $(La_{1-x}Nd_x)_{0.7}Ca_{0.3}MnO_3$, (b) $(La_{1-x}Gd_x)_{0.7}Ca_{0.3}MnO_3$ and (c) $(La_{1-x}Y_x)_{0.7}Ca_{0.3}MnO_3$.

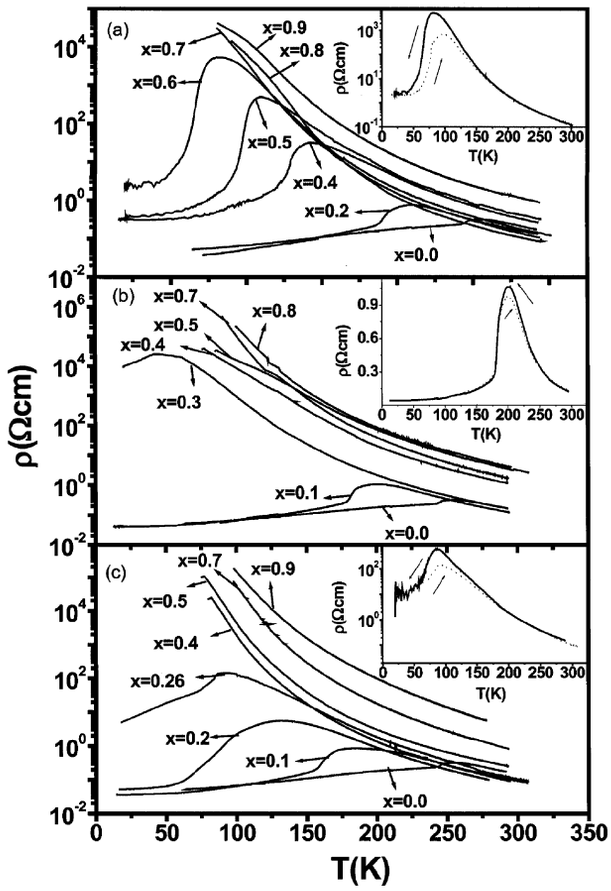

Fig. 3 Temperature variation of the electrical resistivity in (a) $(La_{1-x}Nd_x)_{0.7}Ca_{0.3}MnO_3$, (b) $(La_{1-x}Gd_x)_{0.7}Ca_{0.3}MnO_3$ and (c) $(La_{1-x}Y_x)_{0.7}Ca_{0.3}MnO_3$. The curves in the insets show warming cycle data.

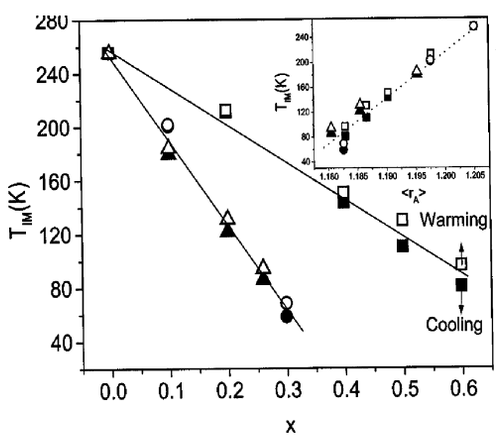

Fig. 4 Variation of T_{IM} with x in $(La_{1-x}Ln_x)_{0.7}Ca_{0.3}MnO_3$ for $x \leq x_c$. The inset shows the variation of T_{IM} with $\langle r_A \rangle$ (Å) for the same composition range.

In $(La_{1-x}Y_x)_{0.7}Ca_{0.3}MnO_3$, ferromagnetism is seen only for compositions with $x \leq 0.2$, T_C decreasing with increase in x. Compositions with $x > 0.2$ show a gradual increase in the μ_B-value below T_M and T_M decreases with increase in x (Fig. 2(c)). Thus, the x_c-value of $(La_{1-x}Ln_x)_{0.7}Ca_{0.3}MnO_3$ is 0.75, 0.6, 0.3 and 0.2 for Ln = Pr, Nd, Gd and Y respectively, showing a sensitive dependence of x_c on $\langle r_A \rangle$.

The magnetization data for $(La_{1-x}Ln_x)_{0.7}Ca_{0.3}MnO_3$ with Ln = Nd, Gd and Y in the compositions range $x \geq x_c$ show certain features of significance. Thus, we find that for the compositions less than or close to x_c, the low-temperature μ_B-value is significant, reaching values anywhere between 1 and 2.5. When x is very large ($x \gg x_c$), the μ_B-value decreases to values less than unity. When Ln = Y, the highest value of ~1μ_B is observed when $x \sim x_c$ (Fig. 2(c)). The drastic change in the values of μ_B around x_c in the three series of manganates with constant carrier concentration can be attributed to phase separation due to disorder caused by substitution of the smaller rare-earth cations in place of La. In the Pr system, phase separation has been reported in the regime of $x \sim x_c$ ($x \sim 0.6$–0.8).[10] To some extent, the results found here are somewhat comparable to those of de Teresa *et al.*[13] who find FMM behaviour at low x and spin-glass behaviour at large x (≥0.33) in $(La_{1-x}Tb_x)_{0.67}Ca_{0.33}MnO_3$.

The electrical resistivity data for $(La_{1-x}Ln_x)_{0.7}Ca_{0.3}MnO_3$ (Ln = Nd, Gd, Y) reflect the magnetization data, with the $x \leq x_c$ compositions showing IM transitions (Fig. 3). The compositions with $x > x_c$ are insulating and do not exhibit IM transitions. For $x \leq x_c$, the value of the resistivity at the IM transition increases with increase in x, and a change in the resistivity of 3–4 orders of magnitude is observed at the transition. Thus, the value of resistivity at 20 K for $x \sim x_c$ is considerably higher than that for $La_{0.7}Ca_{0.3}MnO_3$. The temperature of the IM transition, T_{IM}, for $x \leq x_c$ compositions decreases linearly with increasing x (Fig. 4). The T_{IM} *vs.* $\langle r_A \rangle$ plot is linear with a positive slope as expected (inset of Fig. 4). We have not observed any resistivity anomaly at T ($<T_{IM}$) for any of the compositions unlike Uehara *et al.*[9] and Deac *et al.*[14]

The small but finite magnetic moments and relatively large resistivities at low temperatures found in $(La_{1-x}Ln_x)_{0.7}Ca_{0.3}MnO_3$ for Ln = Pr, Nd, Gd and Y around x_c or $\langle r_A{}^c \rangle$ are a consequence of phase separation. Phase separation also causes thermal hysteresis in the resistivity behaviour around the IM transitions (insets in Fig. 3). The insets in Figs. 4(a)–(c) show that the resistivity in the warming cycle is lower than that in the cooling cycle up to a certain temperature beyond which the resistivities in the two cycles merge. Upon cooling the sample below the IM transition, the FMM phase grows at the expense of the AFM insulating phase, causing a decrease in the resistivity value. When the sample is warmed, the insulating phase grows at the expense of the FMM phase, the latter providing the conductive path. The thermal hysteresis in the resistivity

data is therefore due to the percolative conductivity in these manganates, the hysteresis decreasing with increase in $\langle r_A \rangle$ or decrease in x as expected.

Phase separation in the $(La_{1-x}Ln_x)_{0.7}Ca_{0.3}MnO_3$ series of manganates is related to size disorder caused by the substitution of small ions in place of La and we have quantitatively examined the effect of size-disorder in these manganates, in terms of the size variance of the A-site cation radius distribution, σ^2.[3,15] We have examined the electrical and magnetic properties for a series of $(La_{1-x}Ln_x)_{0.7}Ca_{0.3}MnO_3$ with fixed $\langle r_A \rangle$ and variable σ^2. In Fig. 5, we have shown typical plots of the temperature variation of μ_B for the fixed values of $\langle r_A \rangle$ of 1.196 and 1.17 Å. We see a decrease in T_C with increase in σ^2. For $\langle r_A \rangle$ = 1.17 Å the material is not ferromagnetic. The μ_B-values as well as T_M show a marked decrease with increase in σ^2. The resistivity decreases with increase in magnetization, and when $\langle r_A \rangle$ = 1.196 Å, T_{IM} decreases with increase in σ^2.

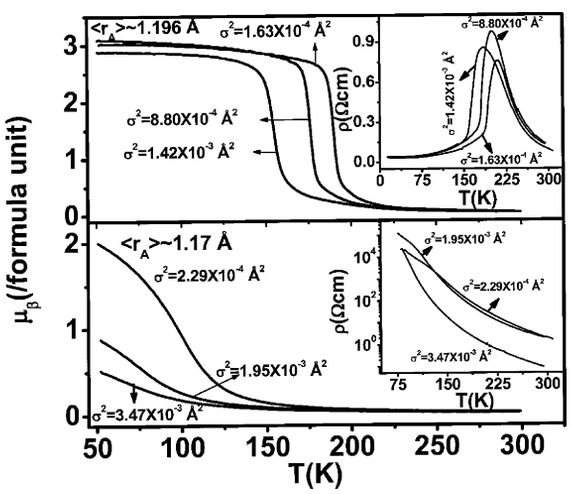

Fig. 5 Temperature variation of μ_B in $(La_{1-x}Ln_x)_{0.7}Ca_{0.3}MnO_3$ with (a) $\langle r_A \rangle$ = 1.196 Å, (b) $\langle r_A \rangle$ = 1.17 Å. The insets show the corresponding variations in resistivities.

Electrical conductivity in the $x \sim x_c$ compositions is percolative at low temperatures and, accordingly, we are able to fit the low-temperature data for the compositions with $\langle r_A \rangle > 1.18$ Å to a percolative scaling law, $\log\rho \propto \log|\langle r_A \rangle - \langle r_A^c \rangle|$, as shown in Fig. 6. The slope of the plot is −2.63, a value close to the experimental and predicted values for percolative systems.[16]

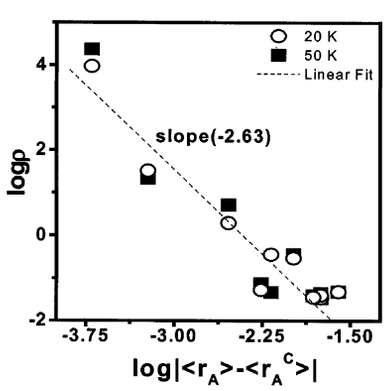

Fig. 6 The linear scaling of $\log\rho$ with $\log|\langle r_A \rangle - \langle r_A^c \rangle|$ for $(La_{1-x}Ln_x)_{0.7}Ca_{0.3}MnO_3$ at 20 and 50 K.

Fig. 7 shows the temperature response of the real part of the dielectric constant (ε') for $(La_{0.3}Y_{0.7})_{0.7}Ca_{0.3}MnO_3$ at different frequencies; ε' reaches high values at ordinary temperatures but decreases dramatically below ~120 K. The unusually high dielectric constant of $(La_{1-x}Ln_x)_{0.7}Ca_{0.3}MnO_3$ for $x > x_c$ can be understood by assuming the presence of conductive domains surrounded by insulating layers with an activated behaviour of

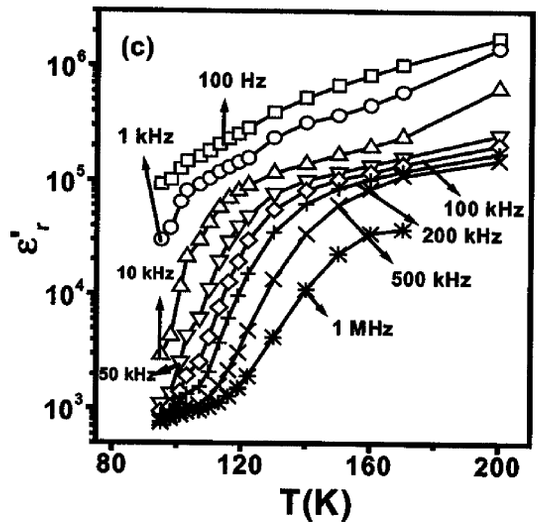

Fig. 7 Temperature variation of the real part of the dielectric constant (ε') of $(La_{0.3}Y_{0.7})_{0.7}Ca_{0.3}MnO_3$ at different frequencies.

the intra-domain (non-percolative) conductivity. Such a finite conductivity could be one of the reasons for the high dielectric constant beyond 120 K.

In Fig. 8 we show the magnetization and resistivity data of $La_{0.7-x}Dy_xSr_{0.3}MnO_3$. The T_C values decrease with increasing x up to a composition $x_c \sim 0.4$. The value of T_C decreases from 350 K for $x = 0.0$ to ~110 K for $x = 0.4$. The abrupt change in magnetization of $La_{0.7-x}Dy_xSr_{0.3}MnO_3$ is noteworthy. There is a small increase in the magnetization at low temperatures (≤80 K) in the $x > x_c$ compositions (Fig. 8(a)), but this is not due to long range FM ordering. If these compositions were FM the T_C value would be expected to be much higher based on the $\langle r_A \rangle$ value. When $x > x_c$, the materials are no longer FM and accordingly, the resistivity increases with the decrease in temperature, as in an insulator (Fig. 8(b)). At large x ($x > x_c$) $La_{0.7-x}Dy_xSr_{0.3}MnO_3$ ceases to exhibit ferromagnetism and IM transition, and instead becomes an insulator with a small increase in magnetization at low temperature indicating that the FM clusters occur in a paramagnetic matrix. The large change

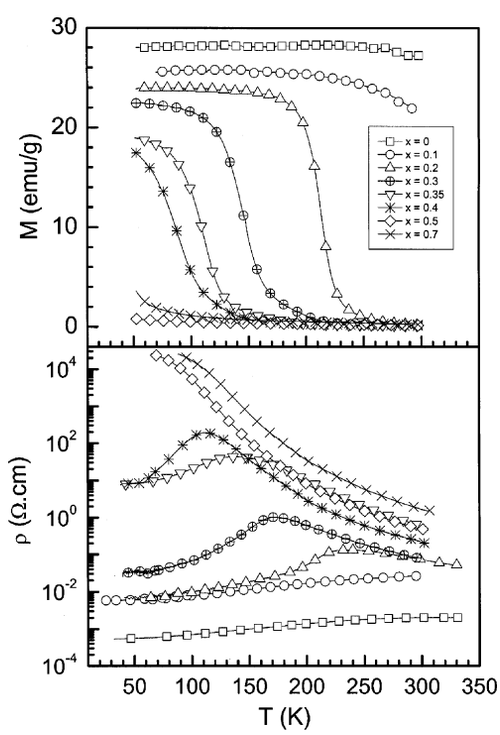

Fig. 8 Temperature variation of (a) magnetization and (b) resistivity of $La_{0.7-x}Dy_xSr_{0.3}MnO_3$.

in the properties around x_c reflects the presence of electronic phase separation in the Sr substituted manganate compositions as well.

$Nd_{0.5}Sr_{0.5}MnO_3$

The occurrence of a phase separated state below T_{CO} (T_N) in some of the manganate compositions was pointed out earlier. The situation is even more complex in $Nd_{0.5}Sr_{0.5}MnO_3$. High-resolution X-ray and neutron diffraction investigations show that $Nd_{0.5}Sr_{0.5}MnO_3$ separates into three macroscopic phases at low temperatures.[17] The phases involved are the high-temperature FMM phase, the orbitally ordered A-type AFM phase, and the charge-ordered CE-type AFM phase. On cooling the manganate, the A-type AFM phase starts manifesting itself around 220 K, with the charge-ordered AFM phases appearing at 150 K. At the so-called FM metallic–CO AFM transition, all the three phases coexist, and this situation continues down to very low temperatures as shown in Fig. 9. In Fig. 10 we show the percentage volume fraction of the different phases in the presence and absence of a magnetic field.[18] Phase separation in this system seems to depend crucially on the Mn^{4+}/Mn^{3+} ratio, a ratio slightly greater than unity stabilizes the A-type AFM phases. Thus, $Nd_{0.45}Sr_{0.55}MnO_3$ has the A-type AFM structure.

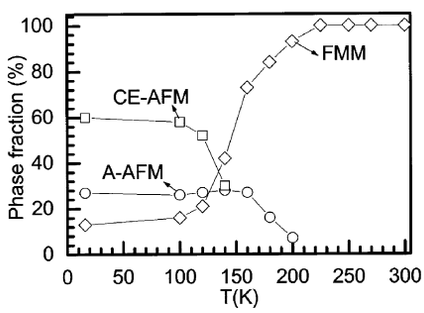

Fig. 9 Variation in the percentage of the different phases of $Nd_{0.5}Sr_{0.5}MnO_3$ with temperature.

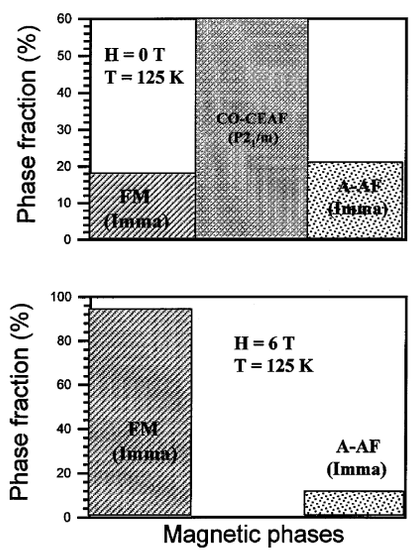

Fig. 10 Schematic diagram of the percentage volume fractions of different phases of $Nd_{0.5}Sr_{0.5}MnO_3$ under (a) $H = 0$ T and (b) 6 T.

Fig. 11 shows the data plotted on T_C and T_{CO} values in the $La_{0.5-x}Ln_xCa_{0.5}MnO_3$ (Ln = Pr, Nd) and $Nd_{0.5}Ca_{0.5-x}Sr_xMnO_3$ series against $\langle r_A \rangle$. Although there is some scatter in the points, the data indicate that when $\langle r_A \rangle \sim 1.20$ Å, the $T_C < T_{CO}$, suggesting that the ferromagnetic transition is re-entrant in nature.[19] Furthermore, the $T_C - \langle r_A \rangle$ and $T_{CO} - \langle r_A \rangle$ curves cross each other around $\langle r_A \rangle = 1.20$ Å. It is likely that over the entire $\langle r_A \rangle$ range 1.17–1.24 Å, there is co-existence of the CO and FM phases, especially in the temperature range between T_{CO} and T_C.

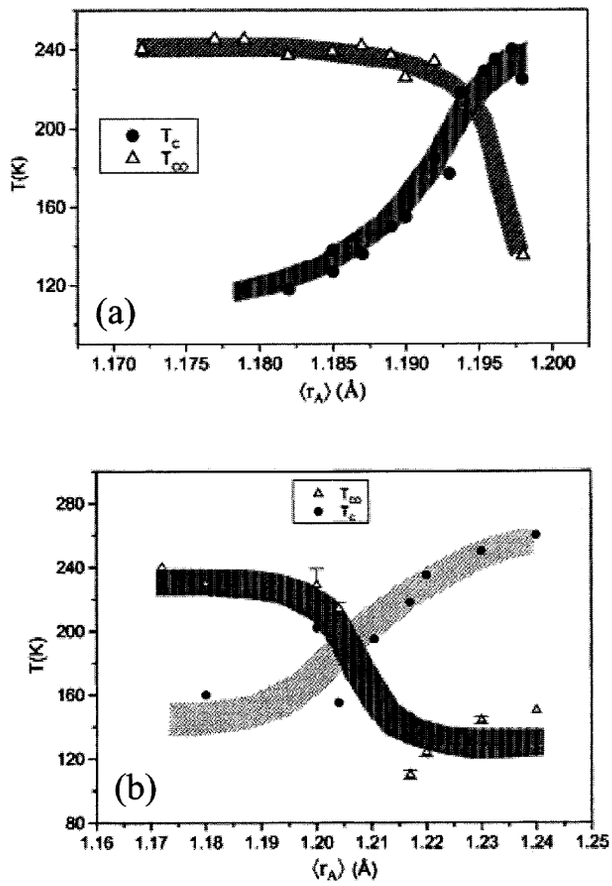

Fig. 11 Variation of the FM Curie temperature, T_C, and the charge ordering transition temperature, T_{CO}, with $\langle r_A \rangle$ in (a) $La_{0.5-x}Ln_xCa_{0.5}MnO_3$ (Ln = Pr, Nd) and (b) $Nd_{0.5}Ca_{0.5-x}Sr_xMnO_3$.

$Pr_{1-x}Ca_xMnO_3$ ($x = 0.3$–0.4)

Based on neutron scattering and diffraction studies, Radaelli *et al.*[4,5] have shown tunable mesoscopic phase separation in $Pr_{0.7}Ca_{0.3}MnO_3$. Intragranular strain-driven mesoscopic phase separation (5–20 nm) between two insulating phases (one charge-ordered and another spin-glass) occurs below T_{CO}. The charge-ordered phase orders antiferromagnetically and the other remains a spin-glass. On the application of a high magnetic field, most of the material goes to a FM state. Microscopic phase separation (0.5–2 nm) is present at all temperatures, especially in the spin-glass phase at low temperatures. Electric fields produce interesting effects on $Pr_{0.6}Ca_{0.4}MnO_3$ and similar CO manganates. In Fig. 12, we show the effect of electric currents on the resisitivity of $Pr_{0.6}Ca_{0.4}MnO_3$ and $Nd_{0.5}Ca_{0.5}MnO_3$ crystals when the sample is cooled from 300 to 15 K. There are four distinct features in the plots. There is a drop in the resistivity throughout the temperature range as the current, I, is increased. The temperature dependence of resistivity changes with the increase in I. An insulator–metal transition occurs

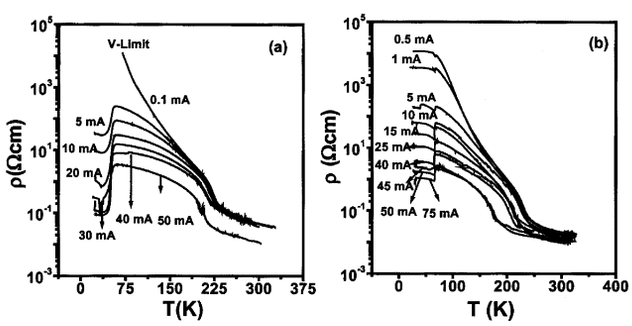

Fig. 12 Temperature variation of electrical resistivity of (a) $Pr_{0.6}Ca_{0.4}MnO_3$ and (b) $Nd_{0.5}Ca_{0.5}MnO_3$ for different values of current.

around 60 K (T_{IM}) at high values of I, beyond a threshold value. The change in the resistivity is not due to Joule heating as evidenced from the negative thermal coefficient of resistivity at high temperatures and the change in sign at the IM transition.[6–8] The negative differential resistance, *i.e.* the decrease in resistivity with increase in current observed beyond a certain value of I (Fig. 12), is due to the presence of the metallic filaments, which are ferromagnetic and carry most of the current.[6] The rather high value of the resistivity below the transition temperature is attributed to the co-existence of the FM and CO insulator phases. The relative fraction of the FMM phase increases with increasing current causing a lowering of resistivity below the T_{IM}.[7,8] The small rise in resistivity below the IM transition may be attributed to the tunneling of electrons between the FMM clusters through COI clusters.

Rare-earth cobaltates

Preliminary measurements (at 1 kOe) of the dc magnetic susceptibilities of $Ln_{0.7}Ca_{0.3}CoO_{3-\delta}$ with Ln = La, Pr, Nd showed that while $La_{0.7}Ca_{0.3}CoO_{2.97}$ clearly exhibits a ferromagnetic transition (T_C ~175 K), $Pr_{0.7}Ca_{0.3}CoO_3$ and $Nd_{0.7}Ca_{0.3}CoO_{2.95}$ do not show distinct ferromagnetic transitions down to 50 K (Fig. 13(a)). There is a slight increase in the susceptibility of $Pr_{0.7}Ca_{0.3}CoO_3$ around 75 K, but this is not due to a genuine ferromagnetic transition. On the basis of the $\langle r_A \rangle$ values, the ferromagnetic T_C's of $Pr_{0.7}Ca_{0.3}CoO_3$ and $Nd_{0.7}Ca_{0.3}CoO_3$ would be expected to be well above 100 K. Electrical resistivities of these cobaltates are also much higher (Fig. 13(b)). The magnetism in the cobaltates is due to Co^{3+}–O–Co^{4+} superexchange, but most of the $Ln_{1-x}A_xCoO_3$ also seem to show evidence for some frustration, as though there is no long-range ferromagnetism. In order to understand the nature of these materials, we have investigated the magnetic properties of $Pr_{0.7}Ca_{0.3}CoO_3$ in detail, down to low temperatures.

In Fig. 14(a) we show the temperature variation of the dc magnetic susceptibility of $Pr_{0.7}Ca_{0.3}CoO_3$ in the zero-field-cooled (ZFC) and field-cooled (FC) states (H = 100 Oe). There

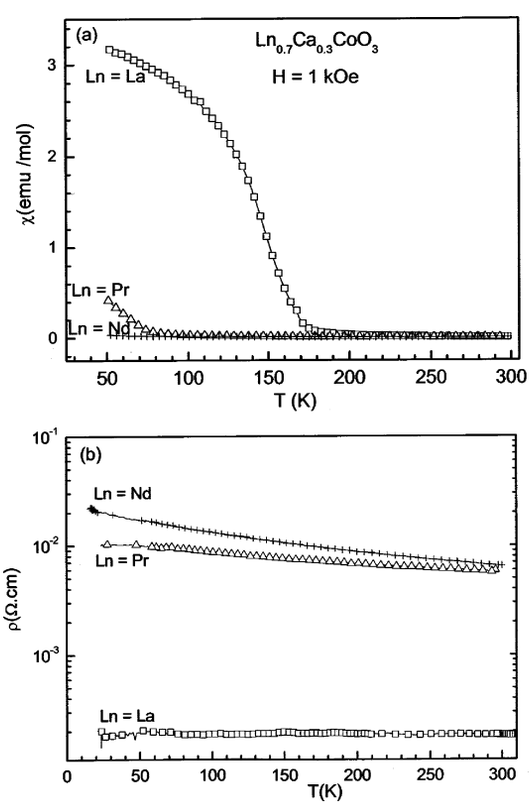

Fig. 13 Temperature dependence of (a) the magnetic susceptibility, χ (H = 1000 Oe) and (b) the electrical resistivity, ρ, of $Ln_{0.7}Ca_{0.3}CoO_{3-\delta}$ (Ln = La, Pr or Nd).

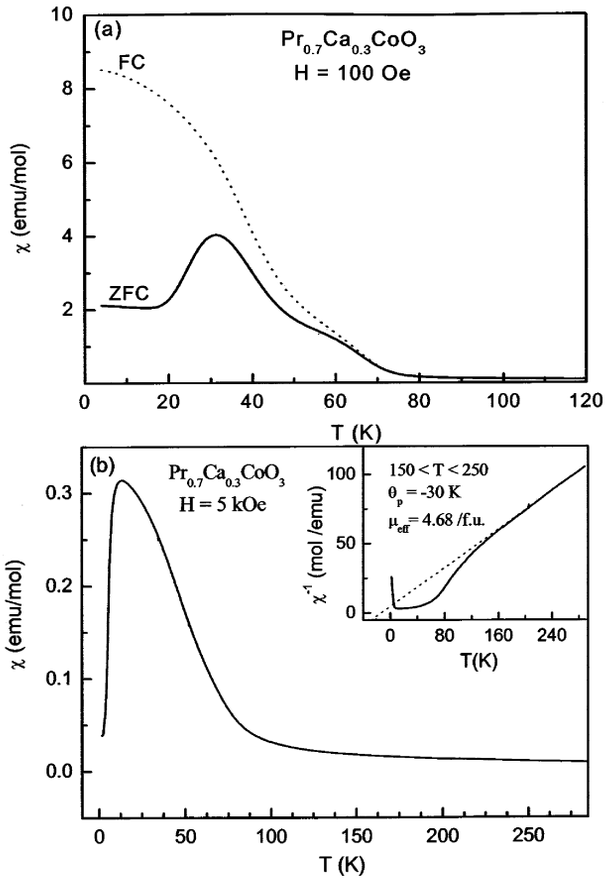

Fig. 14 Temperature dependence of magnetic susceptibility, χ, of $Pr_{0.7}Ca_{0.3}CoO_3$ under (a) H = 100 Oe; solid and dotted lines represent zero-field-cooled (ZFC) and field-cooled (FC) data, respectively, and (b) H = 5000 Oe, the inset shows the temperature dependence of inverse magnetic susceptibility, χ^{-1}.

is considerable divergence in the ZFC and FC behaviour just as in magnetically frustrated systems.[20] The data show two broad transitions around 60 and 30 K. Measurements carried out at 5 kOe, however, do not reveal the two peaks (Fig 14(b)), suggesting that the intermediate temperature range M–H behaviour of this material is rather complex at low fields. The data in Fig. 14(b) suggest that magnetic ordering sets in around 75 K with the susceptibility going through a broad maximum around 15 K. Inverse magnetic susceptibility data, shown in the inset of Fig. 14(b), yield a Curie temperature (θ_p) of −30 K. The high-temperature linear region of the inverse susceptibility data gives a magnetic moment of 4.7μ_B (theoretical value for high-spin Co^{3+}/Co^{4+}, 5.4–5.9μ_B). The low value is likely to be because the Co^{3+}/Co^{4+} ions are partly in the intermediate spin states.[21] The shape of the χ–T plot below 75 K is rather complex, unlike that of ferromagnets. It appears as though there is a spread of magnetic transition temperatures due to local environmental effects.

The M–H behaviour of $Pr_{0.7}Ca_{0.3}CoO_3$ is rather complex especially in the temperature range of 25–60 K. The plots remain nonlinear up to 120 kOe even at 5 K. The behaviour is unlike of ferromagnets and is somewhat comparable to that of frustrated systems. Extrapolation of the M–H data in the high field region to zero field gives a saturation moment of around 0.4μ_B. The small value of the moment on cobalt in the apparently ferromagnetic state, compared with the value in the paramagnetic state, indicates itinerant ferromagnetism, which is possible because the material is conducting. We observe magnetic hysteresis at 5 K even at low fields, suggesting a ferromagnet-like behaviour. The width of the hysteresis loop decreases markedly with increasing temperature. These results reveal that ferromagnetic and antiferromagnetic interactions coexist at low temperatures, with the small conducting ferro-

magnetic domains or clusters giving rise to a small magnetic moment.

ac Susceptibility measurements show that the low-temperature transition has a frequency dependence of about 1.3 K, as the frequency is increased from 1.3 to 1330 Hz (Fig. 15). The 60 K peak, however, shows little shift. The position of the low-temperature peak in the ac susceptibility data at 1.3 Hz, for which the field of measurement is 1 Oe, occurs at 37.4 K, and shifts to lower temperatures at higher fields. Thus, for $H = 100$ and 5000 Oe, the peak occurs at 31.5 and 12.7 K, respectively. Because of the inhomogeneous nature, it is difficult to clearly assign one temperature for the bulk transition in this cobaltate, although the first transition clearly occurs around 60 K. While we have compared the inhomogeneous nature of $Pr_{0.7}Ca_{0.3}CoO_3$ at low temperatures to that of cluster or spin-glasses,[20] isothermal remnant magnetization measurements in the 5–60 K range rule out that the material is actually a glass. Thus, isothermal remnant magnetization is time-independent and does not decay logarithmically or exponentially. It thus appears that $Pr_{0.7}Ca_{0.3}CoO_3$ represents a special case of electronic phase separation.

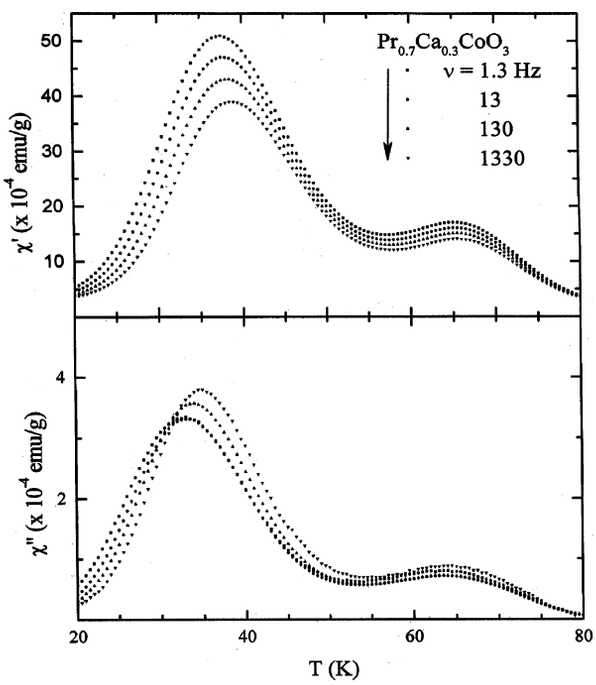

Fig. 15 ac-Magnetic susceptibility data of $Pr_{0.7}Ca_{0.3}CoO_3$ at 1 Oe.

The electronic phase separation and associated magnetic properties of $Pr_{0.7}Ca_{0.3}CoO_3$ and $Nd_{0.7}Ca_{0.3}CoO_{2.95}$ arise because of the small average size of the A-site cations. In these two cobaltates, the average radius (for orthorhombic structure) is less than 1.18 Å, which is the critical value only above which long-range ferromagnetism manifests itself.[11] It is known that increase in size disorder and decrease in size favour phase separation.

Rare-earth cobaltates of the type $Ln_{0.5}A_{0.5}CoO_3$ (Ln = rare earth, A = alkaline earth), especially those with A = Sr are, by and large, ferromagnetic with some of them exhibiting metallic behaviour.[22–25] These properties arise because of the presence of Co^{3+}–O– Co^{4+} states in these cobaltates. The ferromagnetic T_C increases with the increase in the size of the A-site cations. When A = Ba, ferromagnetism occurs when Ln = La (T_C = 190 K) and Nd (T_C = 130 K), but when Ln = Gd, the material shows unusual magnetic and electrical properties. Thus, $Gd_{0.5}Ba_{0.5}CoO_3$ which is charge-ordered at room temperature, shows an increase in magnetization around 280 K, without ever reaching a high value of the magnetic moment.[26–29] Furthermore, $Gd_{0.5}Ba_{0.5}CoO_3$ is an insulator, unlike $La_{0.5}Ba_{0.5}CoO_3$ which is metallic. The average radius of the A-site cations, $\langle r_A \rangle$, as well as the size-disorder arising from the cation size mismatch, as measured by the variance σ^2, are known to play important roles in determining the properties of rare-earth manganates and cobaltates.[3,29] It appears that the large value of σ^2 in the $Gd_{0.5}Ba_{0.5}CoO_3$ (0.033 Å^2) compared to that of $La_{0.5}Ba_{0.5}CoO_3$ (0.016 Å^2) could be responsible for the absence of ferromagnetism and metallicity in the former.[29]

In order to study the effects of cation size, we have examined the magnetic and electrical properties of several series of cobaltates. We show the magnetization and resisitivity data of $Gd_{0.5-x}Nd_xBa_{0.5}CoO_{3-\delta}$ in Fig. 16. With increase in x, we observe the evolution of ferromagnetism. What is interesting is that the 280 K magnetic transition of $Gd_{0.5}Ba_{0.5}CoO_{2.9}$ disappears even when $x \geq 0.1$. When Ln = Nd, we observe a complex behaviour for $x = 0.1$, with a magnetic transition around 220 K. We observe no obvious magnetic transitions in the 200–280 K region for $0.1 < x < 0.4$. The $x = 0.3$ composition shows a small increase in magnetization around 125 K, and the increase becomes more marked when $x = 0.4$. When Ln = La, there is no magnetic transition in the 200–280 K region for $0.1 < x < 0.25$. A distinct FM transition occurs at $x = 0.5$ in the case of Nd, and at $x = 0.4$ in the case of La. It is interesting that the FM characteristics start emerging at low temperatures (<150 K) in these cobaltate compositions around a $\langle r_A \rangle$ value of 1.30 Å. Clearly with an increase in x, the size of ferromagnetic clusters increases, eliminating the phase separation at small x, caused by size disorder. It is noteworthy that in $Pr_{1-x}A_xCoO_3$ ($0 \leq x \leq 0.5$, A = Sr, Ba) spin or cluster glass behaviour has been found at low temperatures.[30] Spin glass behaviour is found in $La_{1-x}Sr_xCoO_3$ ($x < 0.1$), but with increase in x ferromagnetism manifests itself.[31]

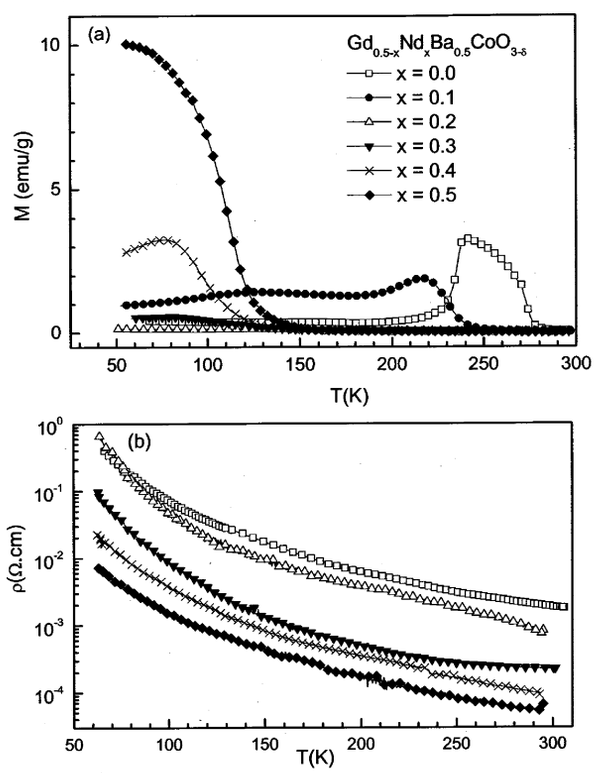

Fig. 16 Temperature variation of (a) the magnetization and (b) the electrical resistivity of $Gd_{0.5-x}Nd_xBa_{0.5}CoO_3$.

The resistivity data of the $Gd_{0.5-x}Nd_xBa_{0.5}CoO_{3-\delta}$ compositions show insulating behaviour, but the resistivity decreases significantly with increase in x, the $x = 0.5$ composition exhibiting the lowest resistivity (Fig 15(b)). When Ln = La, the resistivity decreases with increase in x, becoming temperature-

independent for $x = 0.5$. All the other compositions are insulating. Considering that with an increase in x, there is significant increase in $\langle r_A \rangle$ in the two $Gd_{0.5-x}Ln_xBa_{0.5}CoO_{3-\delta}$ (Ln = La, Nd) series of cobaltates, the changes observed can essentially be attributed to the effects of cation size.

In order to understand the role of size-disorder due to cation size mismatch, we have investigated two series of cobaltates with fixed $\langle r_A \rangle$ values of 1.317 and 1.289 Å, corresponding to those of $Nd_{0.5}Ba_{0.5}CoO_3$ and $Gd_{0.5}Ba_{0.5}CoO_3$. The data for a fixed $\langle r_A \rangle$ of 1.317 Å, show that the T_C decreases as σ^2 increases, eventually destroying the ferromagnetism at a high value of σ^2 (≈0.024 Å^2). The data in Fig 16(a), corresponding to a fixed $\langle r_A \rangle$ of 1.289 Å, are interesting. With decrease in σ^2, the magnetic behaviour of this system changes markedly. Thus, when $\sigma^2 = 0.028$ Å^2, we do not see the magnetic anomaly of $Gd_{0.5}Ba_{0.5}CoO_{2.9}$ at 280 K. When $\sigma^2 = 0.021$ Å^2, we observe a ferromagnetic transition with a T_C of ~160 K. When σ^2 is 0.018 Å^2, the T_C reaches 220 K, a value higher than that of $La_{0.5}Ba_{0.5}CoO_3$. These data clearly demonstrate that the absence of ferromagnetism in $Gd_{0.5}Ba_{0.5}CoO_3$, as well as its unusual magnetic properties, such as the magnetic anomaly at 280 K, are almost entirely due to the disorder arising from the cation size mismatch. Such size-disorder can give rise to electronic phase separation as in the rare-earth manganates.[11,16,32]

The electrical resistivity behaviour of the two series of cobaltates with fixed $\langle r_A \rangle$ values corroborate the results from the magnetic measurements. In Fig. 17(b), we show the resistivity data to demonstrate how the resistivity increases with increase in σ^2. Interestingly, we observe disorder-induced insulator–metal transitions in both the series of cobaltates, the cobaltate compositions with $\sigma^2 < 0.02$ Å^2 showing metallic behaviour. While disorder-induced metal–insulator transitions are common, size variance-induced insulator–metal transitions are indeed novel.

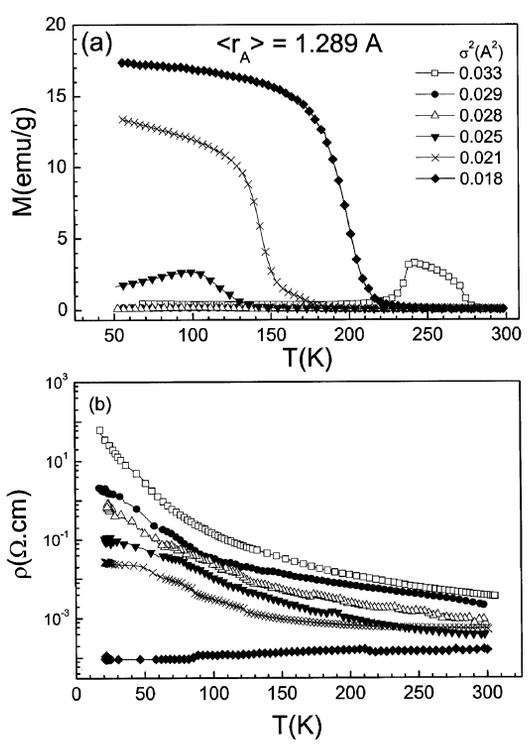

Fig. 17 Temperature variation of (a) the magnetization and (b) the electrical resistivity of $Ln_{0.5-x}Ln'_xA_{0.5-y}A'_yCoO_{3-\delta}$ with a fixed $\langle r_A \rangle$ value of 1.289 Å.

Further support for the observation that cation size-disorder crucially determines the properties of $Gd_{0.5}Ba_{0.5}CoO_{2.9}$ is provided by our study of the $Gd_{0.5}Ba_{0.5-x}Sr_xCoO_{3-\delta}$ series of cobaltates. Here, the $x = 0.5$ composition, corresponding to $Gd_{0.5}Sr_{0.5}CoO_3$, has a smaller $\langle r_A \rangle$ than $Gd_{0.5}Ba_{0.5}CoO_{2.9}$, and yet it shows ferromagnetic features. The 280 K magnetic anomaly of $Gd_{0.5}Ba_{0.5}CoO_3$ disappears even when $x = 0.1$ and the apparent T_C increases with increase in x in the series. This behaviour is clearly due to size disorder, since σ^2 decreases with increase in x. Accordingly, this system exhibits an insulator–metal transition with increase in x or decrease in σ^2. It appears that a σ^2 value larger than 0.02 Å^2 generally destroys ferromagnetism in the cobaltates and changes the metal into an insulator.

That the electrical and magnetic properties of $Gd_{0.5}Ba_{0.5}CoO_3$ are controlled by cation size-disorder is supported by our preliminary studies of $Dy_{0.5}Ba_{0.5}CoO_{2.91}$, with a σ^2 value of 0.037 Å^2. $Dy_{0.5}Ba_{0.5}CoO_{2.91}$ shows a sharp increase in magnetization around 290 K and an antiferromagnetic type transition at 255 K. The general features of the Dy compound are thus similar to those of the Gd compound, except for the higher transition temperatures. The larger size-disorder and associated phase separation in $Dy_{0.5}Ba_{0.5}CoO_{2.91}$ could cause such differences.

Concluding remarks

The discussion in the earlier sections clearly brings out the varied effects of electronic phase separation in the rare-earth manganates and cobaltates. It appears that the phenomenon is much more common than anticipated, to the extent that some workers suggest that even the insulator–metal transition of $La_{0.7}Ca_{0.3}MnO_3$, showing colossal magnetoresistance, is a consequence of phase separation.[2] It is possible that the electron–hole asymmetry in the manganates[33] may also be partly due to phase separation. It is noteworthy that the large changes caused by electromagnetic fields in charge-ordered manganates may indeed be due to electronic phase separation. It would be worthwhile to study the relevance of this phenomenon to other transition metal oxide systems.

Acknowledgements

The authors thank BRNS (DAE), India, for support of this research. A. K. K. thanks University Grants Commission and M. M. S. thanks Council of Scientific and Industrial Research, India, for a fellowship award.

References

1 *Colossal Magnetoresistance, Charge-Ordering and Related Properties of Manganese Oxides*, ed. C. N. R. Rao and B. Raveau, World Scientific, Singapore, 1998; C. N. R. Rao, A. Arulraj, A. K. Cheetham and B. Raveau, *J. Phys.: Condens. Matter*, 2000, **12**, R83; Y. Tokura, *Colossal Magnetoresistive Oxides*, Gordon and Breach, New York, 2000; A. P. Ramirez, *J. Phys.: Condens. Matter*, 1997, **9**, 8171; C. N. R. Rao, A. K. Cheetham and R. Mahesh, *Chem. Mater.*, 1996, **8**, 2421; C. N. R. Rao, *Chem. Eur. J.*, 1996, **2**, 1499.
2 E. Dagotto, T. Hotta and A. Moreo, *Phys. Rep.*, 2001, **344**, 1; A. Mareo, S. Yunoki and E. Dagotto, *Science*, 1999, **283**, 2034; E. L. Nagaev, *Phys.-Usp*, 1996, **39**, 781; E. Dagotto, *Nanoscale Phase Separation and Colossal Magnetoresistance: The Physics of Manganites and Related Compounds*, Springer-Verlag, Berlin, New York, 2003.
3 L. M. Rodriguez-Martinez and J. P. Attfield, *Phys. Rev. B*, 1996, **54**, R15622; J. P. Attfield, *Chem. Mater.*, 1998, **10**, 3239.
4 D. E. Cox, P. G. Radealli, M. Marezio and S-W. Cheong, *Phys. Rev., B*, 1998, **57**, 3305.
5 P. G. Radealli, R. M. Ibberson, D. N. Argyriou, H. Casalta, K. H. Andersen, S-W. Cheong and J. F. Mitchell, *Phys. Rev. B*, 2001, **63**, 172419.
6 C. N. R. Rao, A. R. Raju, V. Ponnambalam, S. Parashar and N. Kumar, *Phys. Rev. B*, 2000, **61**, 594.
7 R. C. Budhani, N. K. Pandey, P. Padhan, S. Srivastava and R. P. S. M. Lobo, *Phys. Rev. B*, 2002, **65**, 14429.
8 S. Srivastava, N. K. Pandey, P. Padhan and R. C. Budhani, *Phys. Rev. B*, 2001, **62**, 13868.

9 U. M. Uehara, S. Mori, C. H. Chen and S-W. Cheong, *Nature (London)*, 1999, **399**, 560; P. B. Littlewood, *Nature (London)*, 1999, **399**, 529.
10 A. M. Balagurov, V. Yu. Pomjakushin, D. V. Sheptyakov, V. L. Aksenov, P. Fischer, L. Keller, O. Yu. Gorbenko, A. R. Kaul and N. A. Babushkina, *Phys. Rev. B*, 2001, **64**, 24420.
11 L. Sudheendra and C. N. R. Rao, *J. Phys.: Condens. Mater.*, 2003, **15**, 3029.
12 H. Terashita and J. J. Neumeier, *Phys. Rev. B*, 2001, **63**, 174436.
13 J. M. de Teresa, M. R. Ibarra, J. Garcia, J. Blasco, C. Ritter, P. A. Algarabel, C. Marquina and A. del Moral, *Phys. Rev. Lett.*, 1996, **76**, 3392.
14 I. G. Deac, S. V. Diaz, B. G. Kim, S-W. Cheong and P. Schiffer, *Phys. Rev. B*, 2002, **65**, 174426.
15 P. V. Vanitha, P. N. Santosh, R. S. Singh, C. N. R. Rao and J. P. Attfield, *Phys. Rev. B*, 1999, **59**, 13539.
16 C. N. R. Rao and P. V. Vanitha, *Curr. Opin. Solid State Mater. Sci.*, 2002, **6**, 97.
17 P. M. Woodward, D. E. Cox, T. Vogt, C. N. R. Rao and A. K Cheetham, *Chem. Mater.*, 1999, **11**, 3528.
18 C. Ritter, R. Mahendiran, M. R. Ibarra, L. Morellon, A. Maignan, B. Raveau and C. N. R. Rao, *Phys. Rev. B*, 2000, **61**, R9229.
19 P. V. Vanitha and C. N. R. Rao, *J. Phys.: Condens. Mater.*, 2001, **13**, 11707; Asish K. Kundu, P. V. Vanitha and C. N. R. Rao, *Solid State Commun.*, 2003, **125**, 41.
20 M. Itoh, I. Natori, S. Kubota and K. Matoya, *J. Phys. Soc. Jpn.*, 1994, **63**, 1486.
21 C. N. R. Rao, M. M. Seikh and N. Chandrabhas, *Top. Curr. Chem.*, 2004, **234**, 1.
22 G. H. Jonker and J. H. van Saten, *Physica*, 1953, **19**, 120; J. B. Goodenough and P. M. Raccah, *Phys. Rev.*, 1967, **155**, 932.
23 V. G. Bhide, D. S. Rajoria, C. N. R. Rao, G. R. Rao and V. G. Jadhao, *Phys. Rev. B*, 1975, **12**, 2832.
24 C. N. R. Rao, O. Parkash, D. Bahadur, P. Ganguly and S. Nagabhushana, *J. Solid State Chem.*, 1977, **22**, 353.
25 M. A. Senaris-Rodriguez and J. B. Goodenough, *J. Solid State Chem.*, 1995, **118**, 323.
26 I. O. Troyanchuk, N. V. Kasper, D. D. Khalyavin, H. Szymczak, R. Szymczak and M. Baran, *Phys. Rev. Lett.*, 1998, **80**, 3380.
27 I. O. Troyanchuk, N. V. Kasper, D. D. Khalyavin, H. Szymczak, R. Szymczak and M. Baran, *Phys. Rev. B*, 1998, **58**, 2418.
28 Y. Moritomo, M. Takeo, X. J. Liu, T. Akimoto and A. Nakamura, *Phys. Rev. B*, 1998, **58**, R13334.
29 P. V. Vanitha, A. Arulraj, P. N. Santosh and C. N. R. Rao, *Chem. Mater.*, 2000, **12**, 1666; A. K. Kundu and C. N. R. Rao, *J. Phys.: Condens. Mater.*, 2004, **16**, 415.
30 K. Yoshii, S. Tsutsui and A. Nakamura, *J. Magn. Magn. Mater.*, 2001, **226–230**, 829.
31 K. Yoshii, H. Abe and A. Nakamura, *Mater. Res. Bull.*, 2001, **36**, 1447.
32 E. Dagotto, J. Burgy and A. Moreo, *Solid State Commun.*, 2003, **126**, 9.
33 K. V. Sarathy, P. V. Vanitha, R. Seshadri, A. K. Cheetam and C. N. R. Rao, *Chem. Mater.*, 2001, **13**, 787.